


ORIGINAL ARTICLE

Pairing dual-frequency GPR in summer and winter enhances the detection and mapping of coarse roots in the semi-arid shrubland in China

X. Cui^{1,2} | X. Liu^{1,3} | X. Cao^{1,2} | B. Fan³ | Z. Zhang² | J. Chen^{1,2} | X. Chen^{1,2} | H. Lin³ | L. Guo³ 

¹State Key Laboratory of Earth Surface Processes and Resource Ecology, Faculty of Geographical Science, Beijing Normal University, Beijing, China

²Beijing Engineering Research Center for Global Land Remote Sensing Products, Institute of Remote Sensing Science and Engineering, Faculty of Geographical Science, Beijing Normal University, Beijing, China

³Department of Ecosystem Science and Management, The Pennsylvania State University, State College, Pennsylvania

Correspondence

L. Guo, Department of Ecosystem Science and Management, The Pennsylvania State University, State College, Pennsylvania.
Email: lug163@psu.edu

Funding information

National Natural Science Foundation of China, Grant/Award Numbers: 41571404, 41401378

Abstract

To complement traditional methods of studying coarse roots (>2 mm in diameter) that are often destructive, laborious and point-based, we tested a dual-frequency ground-penetrating radar (GPR) to non-invasively map lateral coarse roots of shrubs (*Caragana microphylla* Lam.) in the sandy soil of a temperate semi-arid shrubland. The dual-frequency GPR system used in this study simultaneously collects data with two antenna frequencies (400 and 900 MHz). The GPR surveys were repeated in a grid (11 × 4.8 m² with a total of 46 survey lines) in summer and winter. Both antenna frequencies and seasonal GPR surveys generated a consistent pattern of the distribution of lateral coarse roots, indicating reliable interpretation of GPR data for coarse roots mapping. The 400 MHz GPR and the winter survey detected more roots in the deeper soil (>0.6 m depth), whereas the 900 MHz GPR and the summer survey detected more in the shallower soil (<0.6 m depth). The higher wave velocity and lower degree of GPR energy attenuation in the frozen soil enhanced the detection of deep coarse roots. Combining root detection results obtained under all conditions revealed a higher distribution density of lateral coarse roots beneath a depression and at the depth of 0.4–0.6 m, but a lower abundance under the intershrub area (i.e. showing the avoidance of intershrub root overlap). These patterns were not evident in GPR images collected using a single frequency antenna in one season. Ground truthing confirmed that pairing GPR data collected at two frequencies improved the detection frequency of the number of lateral coarse roots. More field tests are required to validate the application of repeated dual-frequency GPR surveys to detect and quantify coarse roots in other ecosystems.

Highlights

- The detection of lateral coarse roots by GPR needs to be further improved in field soils.
- Dual-frequency GPR surveys were repeated in summer and winter to enhance coarse roots mapping.
- Combining seasonal dual-frequency GPR data improved detection frequency of the number of roots.
- Topography and intershrub root competition influence the distribution of lateral coarse roots.

KEYWORDS

field condition, geophysics, non-invasive, plant–soil interaction, repeated surveys, root competition, root distribution

1 | INTRODUCTION

Coarse roots (>2 mm in diameter) set up the structural framework for fine roots (<2 mm in diameter) to develop and connect (Deans, 1981) and, thus, influence the uptake and transport of water and nutrients from soil to plants (Millikin & Bledsoe, 1999; Resh, Battaglia, Worledge, & Ladiges, 2003). Coarse roots, especially lateral coarse roots, provide the physical support for the aboveground system of plants (Brassard, Chen, Bergeron, & Pare, 2011; Ennos, 1993; Reubens, Poesen, Danjon, Geudens, & Muys, 2007). At the pedon to hillslope scales, preferential flow via macropores around coarse roots that controls soil water distribution and groundwater recharge (Guo & Lin, 2018) has been frequently observed in forested hillslopes (e.g., Noguchi, Tsuboyama, Sidle, & Hosoda, 1999) and shrubland (e.g., Li, Yang, Li, & Lin, 2009). Coarse roots can penetrate into fractured or weathered bedrock and accelerate bedrock weathering and pedogenesis (Reubens et al., 2007), which further governs landscape evolution on hillslopes and creates permeability in the Critical Zone (Brantley et al., 2017). At the regional scale, coarse roots are the primary route for photosynthate storage in the subsurface, which regulates long-term carbon sequestration (Jackson et al., 1996) and determines ecosystem resilience to the changing environment (Beerling & Berner, 2005). At the landscape to global scales, rooting depth of coarse roots is key to modelling plant productivity and water-energy-carbon exchange between the Critical Zone and the surrounding environment (Fan, Miguez-Macho, Jobbagy, Jackson, & Otero-Casal, 2017). However, field investigation of coarse roots is often destructive and laborious, such as coring, excavation, the profile wall technique and the rhizotron technique. Apart from disturbance to the root zone, results from these point-based measurements are challenging when characterizing the spatial distribution of coarse roots at larger spatial scales (Guo, Chen, Cui, Fan, & Lin, 2013). Geophysical techniques have become a valuable means of non-invasive detection and quantification of coarse roots in the field (al Hagrey, 2007; Jayawickreme, Jobbagy, & Jackson, 2014). Among common geophysical techniques, ground-penetrating radar (GPR) provides the best combination of data acquisition rate, detection depth, spatial coverage and time–space resolution for the detection of coarse roots (Leucci, 2010).

In theory, GPR detects the contrast in dielectric permittivity, a measure of how well the electromagnetic energy is

transmitted through a medium (Jol, 2009). Electromagnetic energy (usually ranging from 10 to 2000 MHz) generated by transmitting antenna propagates into the ground as waves. When radar waves pass across interfaces between media with different dielectric permittivity, a portion of the radar energy is reflected to the receiving antenna, while the remainder continues to penetrate deeper until it is attenuated thoroughly (Jol, 2009). According to the travel time, amplitude, shape and polarity of reflections in GPR images, the location and size of the buried objects can be determined (al Hagrey, 2007). Because water content is the dominant control of dielectric permittivity, GPR wave velocity and reflection strength are sensitive to water variation in the subsurface (Topp, Davis, & Annan, 1980). The relatively higher water content in roots in relation to the surrounding soil creates the necessary contrast in dielectric permittivity and makes root detection by GPR possible (Butnor et al., 2003; Guo, Chen, et al., 2013). For further information on GPR principles and its application in ecohydrology, readers are referred to the reviews by Huisman, Hubbard, Redman, and Annan (2003), Jayawickreme et al. (2014) and Parsekian, Singha, Minsley, Holbrook, and Slater (2015).

So far, GPR has been tested for visualizing the branching patterns of coarse roots (Guo et al., 2015; Zhu, Huang, Su, & Sato, 2014), reconstructing root system architecture and root profiles (Borden, Thomas, & Isaac, 2017; Raz-Yaseef, Koteen, & Baldocchi, 2013; Wu et al., 2014), quantifying root biomass (Butnor et al., 2003; Liu et al., 2018; Molon, Boyce, & Arain, 2017) and measuring root zone soil moisture (Liu et al., 2019). Despite the potential of GPR in root investigation, its successful application, however, highly depends on site-specific conditions and the selection of appropriate GPR systems (Butnor et al., 2003; Guo, Chen, et al., 2013). Some factors influence the performance of GPR-based root detection and quantification, such as field soil conditions (e.g. soil texture, soil organic content and soil water content), root water content, root branching patterns and GPR antenna frequency (Guo, Lin, Fan, Cui, & Chen, 2013; Hirano et al., 2009; Wu, Guo, Li, Cui, & Chen, 2014). For example, a lower antenna frequency offers a deeper penetration depth but a lower spatial resolution, whereas a higher frequency picks up finer structural details but has shallower penetration. The fusion of GPR data collected at a lower frequency and a higher frequency provides high-resolution data with a deeper penetration (e.g. De Coster & Lambot, 2018). Several fusion methods of multifrequency

GPR data have been developed to maximize the detection resolution and the investigation depth of GPR (Hugenschmidt & Kalogeropoulos, 2009; Xiao & Liu, 2015). The recent development of the dual-frequency GPR system provides a new opportunity to address this issue without performing GPR data fusion. A dual-frequency GPR system simultaneously collects data at two centre frequencies (e.g. 900 and 400 MHz or 600 and 200 MHz) over the same survey line, which enhances the reliability in probing structures and processes in both shallow and deep subsurfaces (e.g. Klenk, Jaumann, & Roth, 2015). Therefore, whether the dual-frequency GPR system can promote coarse root detection and mapping is worthy of field tests.

The non-invasive nature of geophysical measurements allows repeated surveys to better visualize subsurface structures and dynamics over time. For instance, repeated GPR surveys after controlled infiltration and irrigation have been used to monitor the evolution of the subsurface flow network in forested hillslopes (e.g. Angermann et al., 2017; Guo, Chen, & Lin, 2014). However, previous GPR root investigation was primarily based on a one-time survey in the growing season, and non-invasive and repeated surveys have not been made good use of. Also, studies of the optimal timing for collecting GPR data to detect and map coarse roots have rarely been conducted. Therefore, whether repeated GPR surveys under different field conditions can help constrain the interpretation of root distribution requires field validations.

To address these issues and further enhance the use of GPR in root investigation, we tested a dual-frequency GPR system that operates at 900 and 400 MHz in a sandy shrubland in summer and winter. We examined the influence of antenna frequency and the time of year on the efficiency of GPR in detecting lateral coarse roots. Then, we evaluated if combining root detection results from two antenna frequencies could improve the detection frequency of lateral coarse roots. **Given the increasing use of geophysical methods for root studies, we expect broader applications of dual-frequency GPR to characterize coarse roots distribution and the complex plant–soil interactions.**

2 | MATERIALS AND METHODS

2.1 | Study site

The study site (43°55'N, 116°12'E; 1,084 m a.s.l.) is located in a semi-arid steppe in Xilingol, Inner Mongolia, north China (Figure 1a). This area has a temperate continental climate, with a mean annual air temperature of 2.6°C and mean annual precipitation of ~300 mm (Yiruhan et al., 2014). The annual potential evapotranspiration is ~1750 mm. The mean July air temperature is 21°C, whereas the corresponding

value for January is -18°C (Chen, Hori, Yamamura, Shiyomi, & Huang, 2008; Chi, Wang, Li, Liu, & Li, 2018). Most of the rainfall occurs in summer, and snowfall mainly occurs from November to March (Zhao, Peth, Wang, Lin, & Horn, 2010).

This region was formed on basalt plateaus and is mantled primarily with fine-sand loess (Hoffmann, Funk, Reiche, & Li, 2011). As formed by aeolian deposits, the soil has relatively homogeneous physiochemical properties (Wu et al., 2015). Local soil texture types are sand and sandy loam (Li et al., 2013), classified as Calcic Kastanozems (FAO) or Calcic Orthic Aridisol (USDA). Average sand, silt and clay content is 47%, 37% and 16%, respectively (Zhao et al., 2010). Bulk density ranges from 1.32 to 1.55 g cm^{-3} (Zhang et al., 2013). These are deep (> 2 m depth), excessively drained, rapidly permeable and low organic content soils (Zhao et al., 2011), which provide suitable conditions for GPR-based root investigation (Guo et al., 2015; Liu et al., 2019).

Grassland degradation and shrub encroachment are taking place in this region because of the changing climate and inappropriate land management (e.g. overgrazing) (Cao et al., 2018). The dominant shrub species is *Caragana microphylla* Lam. Interspersed small mounds associated with *C. microphylla* Lam. colonies dominate the landscape (Figure 1b). The intershrub areas are occupied by perennial grasses; for example, *Stipa krylovii* Roshev., *Leymus chinensis* (Trin.) Tzvel., *Cleistogenes squarrosa* (Trin. ex Ledeb.) Keng and *Artemisia frigida* Willd. (Figure 1c). The growing season lasts from May to September (Ren & Zhang, 2018). *Caragana microphylla* Lam. is selected as the study species, which controls organic carbon sequestration, nitrogen accumulation and the hydrologic cycle in the study area (Cao et al., 2018).

2.2 | GPR survey grid setup

A survey grid ($4.8 \times 11.0 \text{ m}^2$) was established in a relatively flat area on a smooth rolling landscape (slope $< 5^{\circ}$) for root detection and mapping (Figure 1c, d). Four shrub plants (*C. microphylla* Lam.), namely P1 to P4, are distributed within the survey grid. Distance from other shrub plants to the survey grid was over 5 m (Figure 1c, d). Thus, the detected roots were likely to be growing from the shrubs within the survey grid. We measured the size and height of the canopy of the shrubs (Figure 2). To avoid disturbance to shrub growth, we did not set up survey lines across the canopy. The survey grid comprised 14 lines (each 11.0 m long) spaced 0.2 m apart along the southwest to northeast direction, and 32 lines (each 4.8 m long) spaced 0.2 m apart along the southeast to northwest direction (Figure 2). The starting and ending points of survey lines X1, X14, Y1 and Y32 (i.e. boundary survey lines) were anchored into the ground

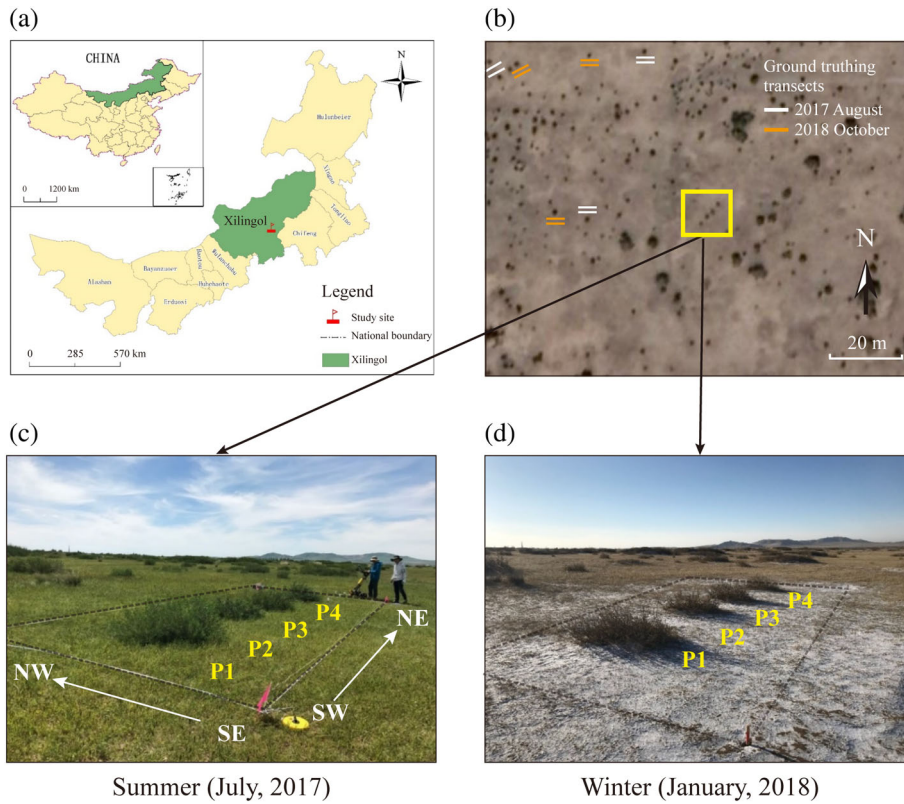


FIGURE 1 (a) The study site is located in Xilingol, Inner Mongolia, north China. (b) This area is semi-arid shrubland with *Caragana microphylla* Lam. as the dominant shrub species. Locations of the GPR survey grid and 12 ground truthing transects are shown. (c, d) Vegetation cover and ground surface condition in summer and winter, respectively. P1–P4 indicates four shrubs (*C. microphylla* Lam.) within the GPR survey area that is defined by the dashed lines. GPR survey directions include southwest (SW) to northeast (NE) and southeast (SE) to northwest (NW)

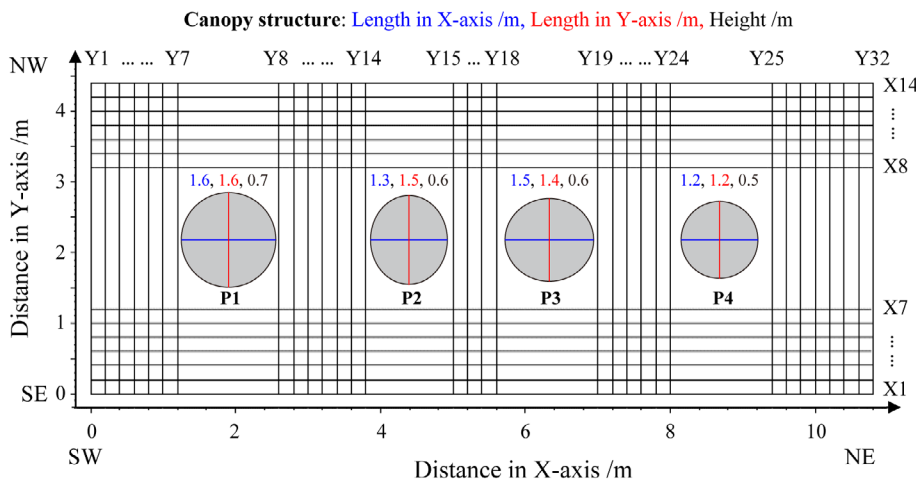


FIGURE 2 The grid layout for GPR surveys. X1–X14 indicates the survey lines along the X-axis (southwest to northeast), and Y1–Y32 the survey lines along the Y-axis (southeast to northwest). P1–P4 indicates the shrubs within the GPR survey grid. The size (length in X- and Y-axis) and height of the canopy of each of the shrubs measured in summer is shown

by plastic stakes to ensure the reproducibility of GPR data (Figure 1c, d). The boundary survey lines were marked every 0.2 m to indicate the starting and ending points of the other survey lines.

2.3 | GPR system and seasonal surveys

We used an IDS GPR system with two pairs of antennae shielded in the same antenna box (RIS MF Hi-Mod; Ingegneria Dei Sistemi Inc., Pisa, Italy). This dual-frequency GPR system simultaneously collects data from the same survey line at two frequencies (900 and 400 MHz). A survey

wheel attached to the antenna box recorded the distance along the survey line. We collected 512 samples per trace at a timestep of 0.0586 (or 0.1172) ns for a total record length of 30 (or 60) ns for the 900 (or 400) MHz antenna. The traces were triggered every 1.6 (or 3.2) cm for the 900 (or 400) MHz antenna along each survey line. The GPR surveys were conducted on July 16, 2017 and January 13, 2018 (Figure 1c, d) to represent the summer and winter conditions, respectively. The litter layer and snow cover were removed from the survey grid before the GPR survey to ensure good coupling between the antenna and the ground surface.

TABLE 1 Average volumetric soil water content (θ) and soil temperature (T) at different depths on experiment days and in two seasons

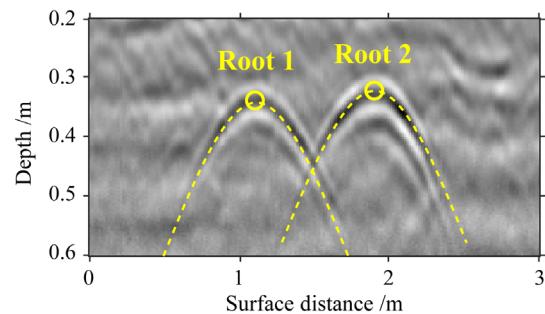
Soil depth (cm)	Summer				Winter			
	Jul. 16, 2017		Average (Jun. to Aug.)		Jan. 13, 2018		Average (Nov. to Jan.)	
	θ (%)	T (°C)	θ (%)	T (°C)	θ (%)	T (°C)	θ (%)	T (°C)
20	6.2	20.7	4.3	19.6	4.1	-14.9	5.1	-8.6
50	7.8	17.7	6.1	16.7	3.5	-12.0	4.8	-5.2
80	6.1	15.2	5.8	14.3	4.2	-10.1	4.6	-2.6
110	5.5	13.8	5.5	12.9	4.4	-7.3	4.3	0.2
150	5.0	10.2	5.2	9.2	4.1	-4.3	4.1	3.1

Five soil moisture probes (ECH2O-5TE; METER Group, Inc., U.S.A.) were installed 0.5 m away from the survey grid at five depths (20, 50, 80, 110 and 150 cm depth). All probes were connected to an EM50 datalogger (METER Group, Inc., Pullman, USA) that recorded soil moisture and temperature every hour. Table 1 lists the average soil water content and soil temperature measured on both experiment days as well as the average value for summer and winter, respectively.

2.4 | Lateral coarse roots detection

The following post-processing steps were performed in Reflex-Win 7.2 (Sandmeier Scientific Software, Germany) to enhance the signal-to-noise ratio in GPR images: (1) first break correction by aligning the first breaks across the traces and first-arrival time zero adjustment; (2) DC drift removal by detrending and dewow filtering; (3) inverse amplitude gain to compensate energy attenuation with propagation depth using the same gain factor in both seasons for consistent comparison; (4) first-order Butterworth filtering to remove both the high-frequency and low-frequency noise; (5) background removal to wipe off antenna reverberation, and (6) travel time to depth conversion using wave velocity calculated from the travel time from the ground surface to a buried reflector at a known depth.

The post-processed GPR images were used for the identification of lateral coarse roots that generate hyperbolic reflections (Guo, Chen, et al., 2013). We used the Randomized Hough Transform (RHT) algorithm proposed by Li et al. (2016) to automatically identify hyperbolic reflections in GPR images (Figure 3). The peak of a hyperbola was considered the location of a lateral coarse root (Liu et al., 2019). As the Xilingol steppe has been a deposition region for aeolian sediments for centuries (Hoffmann et al., 2011), the chance of encountering non-root reflectors (e.g. rocks) in the root zone (0–2 m depth) that can form hyperbolic reflections is very low. These processes were performed with MATLAB (The MathWorks, Inc., Natick, USA). For the detailed description of automatic identification and location

**FIGURE 3** An example of detecting and locating lateral coarse roots by identifying hyperbolic reflections in the GPR image collected over the survey line Y10. The peak of the hyperbola indicates the location of a lateral coarse root

of coarse roots, readers are referred to Li et al. (2016) and Liu et al. (2019).

2.5 | Pairing root distribution derived under different experimental conditions

We first compared the distribution of detected root points in two seasons for the same antenna frequency. To provide an intuitively understandable comparison, all of the detected root points were projected into the two-dimensional (2-D) scale, including the top view and the cross-section view. Further, all of the detected root points in both seasons were plotted together in the 3-D space. We divided the root points into three groups, including roots detected in both seasons, roots only detected in summer and roots only detected in winter. For the i^{th} root point (R_i) detected in summer, a spherical searching window with a diameter of 5 cm and centred at R_i was created in the 3-D space. If multiple root points detected in winter were found in the searching window, the one with the least distance to R_i was considered the same root point (R_i) that was identified again in winter (i.e. detected in both seasons). If no root point appeared in the searching window, R_i was considered detected only in summer. Root points detected in winter that could not be associated with any root

point detected in summer were considered only detected in winter. Then, we combined the root points detected in two seasons into an improved root distribution map, including all of the root points detected in summer plus those only detected in winter. Furthermore, the improved root distribution maps obtained under two antenna frequencies were compared in the 3-D space. In the same procedure described above, root points were divided into those detected by both antenna frequencies, only detected by 900 MHz and only detected by 400 MHz. Finally, root points detected by the 900 MHz GPR and those only detected by the 400 MHz GPR were combined into an optimal root distribution map with the maximized detection frequency of coarse roots.

2.6 | GPR wave velocity

The velocity of the GPR wave in each season was calibrated by hammering a steel rebar into the soil at a depth of 0.35 m in a soil pit 0.5 m from the GPR survey grid, running a GPR scan over the rebar, and picking the corresponding arrival time to the top of the rebar in the GPR images. Change in GPR wave velocity and penetration depth was used to explain the varied efficiencies of GPR in detecting lateral coarse roots between summer and winter.

2.7 | Ground truthing

Ground truthing data were collected from 12 transects (each 5 m long) near the survey grid (Figure 1b), six transects in August 2017 (i.e. the peak of the growing season) and six more in October 2018 (i.e. after the growing season). Each transect was scanned by the dual-frequency GPR and then excavated to the depth of ~1 m to expose and document the distribution of lateral coarse roots (Figure S1). Lateral coarse roots identified in GPR images were compared with those recorded on the corresponding soil profiles to determine the detection frequency of the number of coarse roots (Figure S1). Because of the frozen soil conditions, excavation in winter was impracticable and, thus, ground truthing data were not collected in winter. Further, soil layering patterns were documented in a natural outcropping of soil (2.5 m depth) located ~500 m away from the survey grid. Because soil at the study site was formed by aeolian deposits and with relatively uniform soil layering patterns, the observation on the outcrop can represent the condition of the GPR survey grid.

3 | RESULTS

3.1 | Seasonal signal change in GPR images

The GPR images collected over the same survey line with two antenna frequencies in two seasons are compared in

Figure 4. Two antenna frequencies generate similar GPR reflection patterns, but the 400 MHz GPR penetrates deeper than the 900 MHz GPR in both seasons. Winter conditions promote GPR wave propagation to the deeper soil. The effective detection depth (showing clear reflection patterns that allow the identification of subsurface features) increases from 1 m (or 2 m) in summer to 2.5 m (or 3.5 m) in winter for the 900 MHz (or 400 MHz) GPR. Reflection amplitude at the 0–1-m soil depth also intensifies in winter for both antenna frequencies.

The 900 MHz GPR images capture more detailed subsurface structures than those collected with the 400 MHz GPR, which helps the identification of coarse roots. In summer, 37 root points are identified by the 900 MHz GPR (Figure 4a), but 27 are identified by the 400 MHz GPR (Figure 4c). The 900 MHz GPR also reveals more root points in winter than the 400 MHz GPR (Figure 4b, d). Twenty-five of 37 (or 21 of 27) root points identified in summer are captured again in winter by the 900 MHz (or 400 MHz) GPR. The consistency between seasonal surveys demonstrates the effectiveness of GPR in identifying and mapping lateral coarse roots. For both antenna frequencies, the summer survey reveals more root points in the topsoil (<0.5 m depth; Figure 4a, c), whereas the winter survey reveals more in the deeper soil (0.5–1.5 m depth; Figure 4b, d).

The lower antenna frequency is more effective in differentiating soil layering patterns. Two horizontal reflections are visible in the 400 MHz GPR image collected in winter (Figure 4d), which match with observations on a nearby outcrop of soil (Figure 4e). The shallower interface (~1.5 m depth) is likely to indicate the top of the caliche layer marked by a light colour due to CaCO₃ accumulation, and the deeper interface (~2.5 m depth) shows the transition from the caliche layer to the CR horizon (Tamura, Asano, & Jamsran, 2013). Figure 4d also suggests that the majority of the lateral coarse roots of *C. microphylla* Lam. are distributed above the caliche layer.

3.2 | Root distribution obtained in two seasons

The spatial distribution of lateral coarse roots derived by the 900 MHz GPR is compared between summer and winter in Figure 5. The top view of the distribution pattern of lateral coarse roots is similar between two seasons (Figure 5a, c), demonstrating the reproducibility of root detection results by GPR under different field conditions. The distribution of lateral coarse roots shows preferential proliferation in space in that fewer root points are identified under the intershrub area (Figure 5a, c). The cross-section view indicates that more root points are detected in the deeper soil (>1 m depth) in winter, but the spatial pattern of root distribution is similar in the shallower soil (<1 m depth) between two seasons (Figure 5b, d). It is also

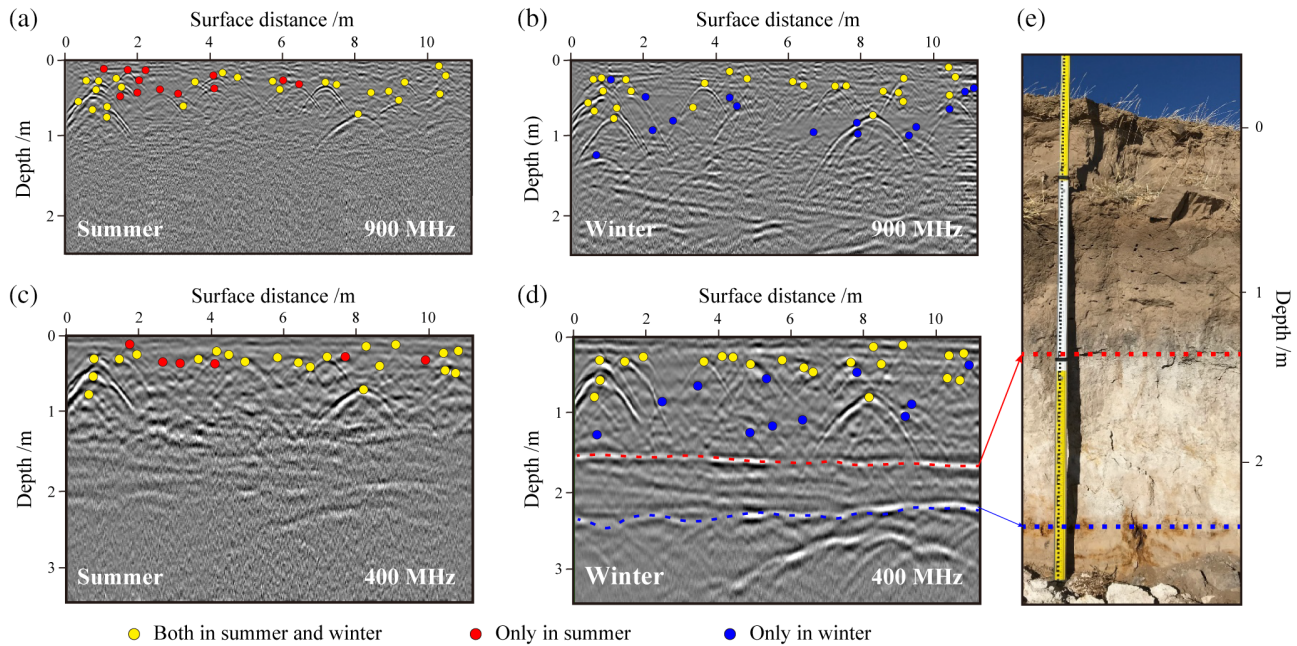


FIGURE 4 Seasonal change in GPR reflection patterns and root detection results. (a, b) GPR images collected by the 900 MHz antenna; (c, d) images by the 400 MHz antenna. (a, c) are collected in summer and (b, d) in winter. All of the GPR images were collected over the same survey line (i.e. X5). For the same antenna frequency, the yellow dots indicate the lateral coarse roots that are identified in both seasons, and the red (or blue) dots indicate the roots that are only identified in summer (or winter). (e) Photograph of a typical soil profile in the study area (~100 m from the GPR survey grid) showing interfaces between soil horizons (indicated by the dashed lines) that are distinguishable in the 400 MHz GPR image collected in winter (d)

noticeable that lateral coarse roots cluster at a depth of ~0.5 m in the soil, and fewer lateral coarse roots are distributed under the canopy (Figure 5b, d). Soil moisture monitoring in summer (June to August) shows that the soil at this depth is the wettest at the study site from the surface to 1.5 m depth (Table 1).

Furthermore, we plot root distribution density against soil depth in both seasons (Figure 6). The 2-D root profile shows that more root points are detected in the shallower soil (<0.6 m depth) in summer with the 900 MHz GPR, whereas more roots are detected in the subsoil (0.6–2 m depth) in winter (Figure 6a). Compared to the 900 MHz GPR, the 400 MHz GPR (Figure 6b) identifies fewer root points from the surface to 1.5 m depth but more in the deeper soil (>1.5 m depth). The 400 MHz GPR captures more root points than the 900 MHz GPR in winter at all depth intervals except for the near-surface layer (0–0.2 m depth). Root profiles obtained with the two antenna frequencies are consistent, both suggesting a unimodal pattern of lateral coarse root density that peaks at a depth of 0.4 to 0.6 m (Figure 6).

Root distribution maps obtained by the 400 MHz GPR in two seasons are compared in Figure 7. Although fewer root points are detected by the 400 MHz GPR than by the 900 MHz GPR, the general pattern of lateral coarse root distribution in both the top view and the cross-section view is similar to that derived by the 900 MHz GPR (Figures 6 and 7). Avoidance of intershrub overlap and the higher density of lateral coarse roots

at a depth of ~0.5 m are also revealed. The consistency between root distribution maps derived by different antenna frequencies and under various field conditions helps robust interpretation of GPR results to map lateral coarse roots.

3.3 | Refined root distribution map by integrating seasonal dual-frequency GPR measurements

We first combine root detection results in both seasons for each antenna frequency (Figures 5e, f and 7e, f). From the top view, both antenna frequencies suggest that more lateral roots are distributed in the lower left, southern corner of the survey grid (Figures 5e and 7e). The survey grid is tilting to the south (Figure 1c, d), making the southern corner the lowest point in topography within the survey grid. As the survey grid is located on a gently rolling slope, water probably converges to this depression after rainfall via overland flow and subsurface lateral flow that leads to a higher soil water content as well as more lateral coarse roots. The cross-section view of the root distribution map (Figures 5f and 7f) suggests that the distribution density of lateral coarse roots increases with the increasing distance from the canopy. In addition, deeper lateral coarse roots (>1 m depth) are primarily found below the midpoint of the intershrub area to avoid intershrub root competition at

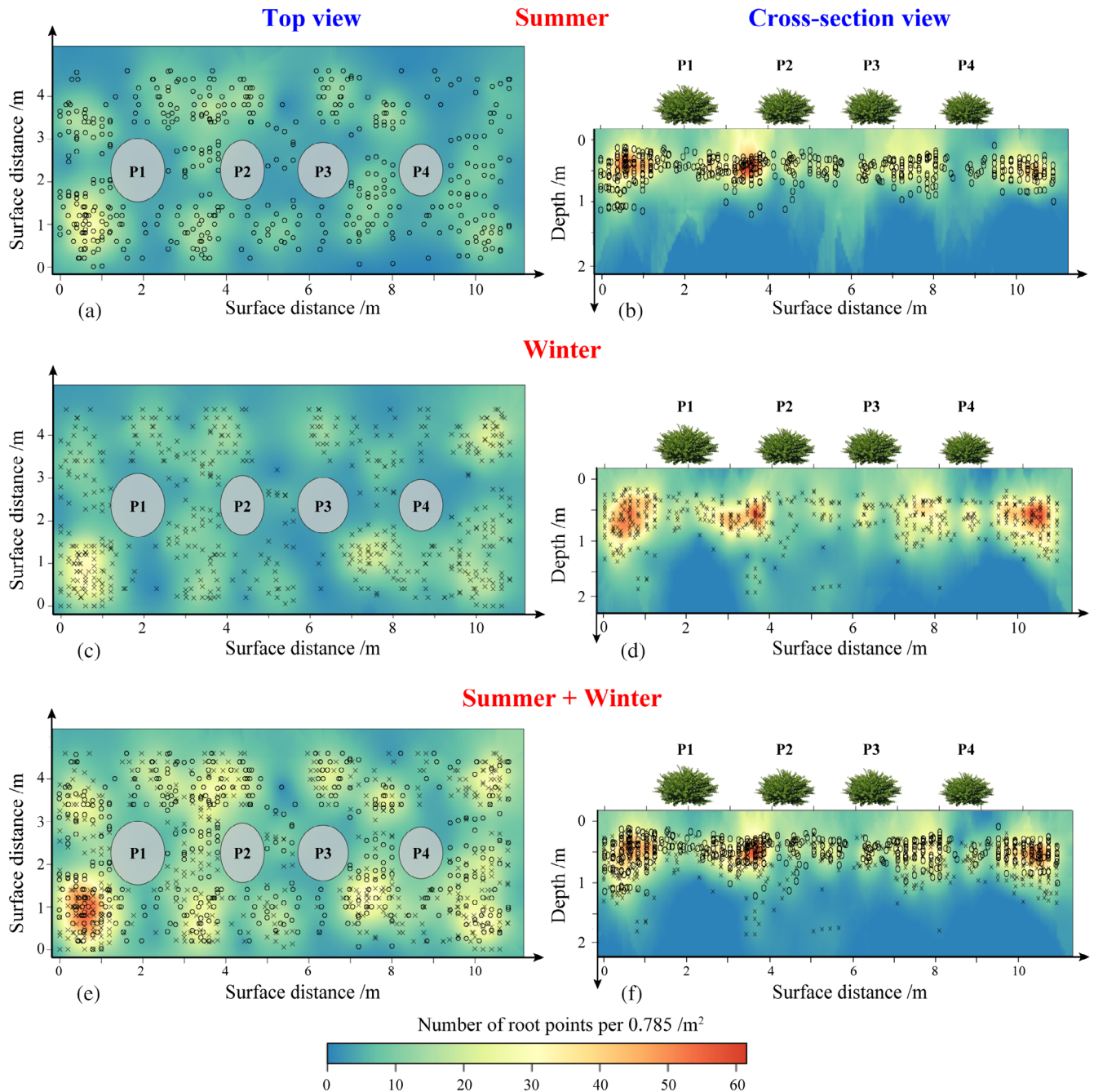


FIGURE 5 Spatial distribution of lateral coarse roots derived by the 900 MHz GPR in summer (a, b) and winter (c, d). The open circles (or crosses) indicate the roots identified in summer (or winter). The base map is the interpolated root distribution density. (e, f) Root distribution map after combining root detection results in summer and winter. Note that roots identified in summer and in both seasons are indicated by the open circles, and the cross marks indicate the roots only detected in winter. (a, c, e) The top view. (b, d, f) The cross-section view. P1–P4 indicates the shrubs within the GPR survey grid

the same depth. The higher abundance of lateral coarse roots below the surface depression area and deeper rooting depth under the intershrub area are more noticeable on root distribution maps after the results of two seasonal surveys are combined (Figures 5e, f and 7e, f) than on those only based on the results of each season (Figures 5a–d and 7a–d).

In addition, we combine root detection results derived by two antenna frequencies in two seasons to obtain the optimal lateral coarse root distribution map (Figure 8a). The winter survey complements the summer survey by adding root points in the deeper soil layer (>1 m depth). The distribution of lateral coarse roots in the 3-D space is clearly anisotropic, which creates the opportunity to link root distribution to

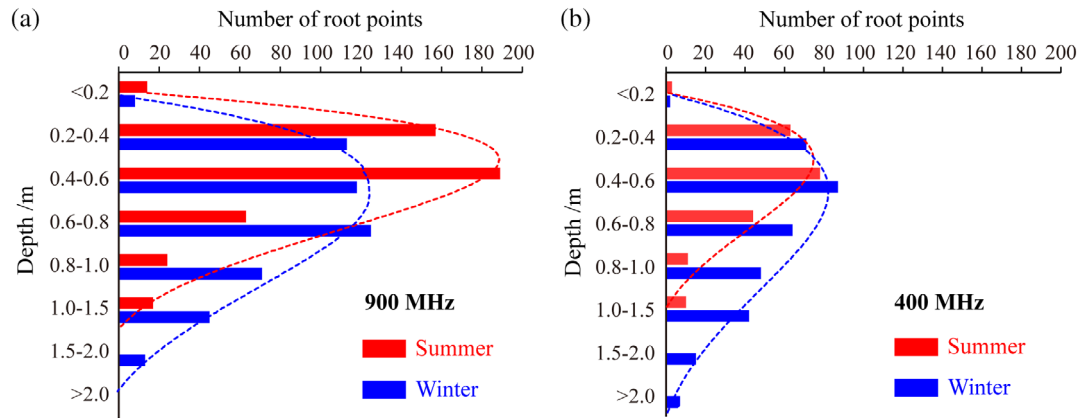


FIGURE 6 A comparison of the vertical distribution of lateral coarse roots obtained in summer and winter. (a) The 900 MHz GPR. (b) The 400 MHz GPR. The number of root points identified in each of the depth intervals and the fitting curves of the vertical distribution of the roots are also shown

edaphic conditions (e.g. soil structure) and biotic factors (e.g. root competition between neighbouring plants). Additionally, an optimal 2-D root profile is obtained (Figure 8b), which can help model the vertical distribution of lateral coarse roots of *C. microphylla* Lam. Integrating root detection results obtained by dual-frequencies GPR in two seasons leads to the maximum number of detected root points (Figure 8b). The 400 MHz GPR or the winter survey complements the 900 MHz GPR or the summer survey by detecting more roots in the deeper soil (Figures 6 and 8), and the 900 MHz GPR or the summer survey complements the 400 MHz GPR or the winter survey by recognizing more root points in the shallower soil (Figures 6 and 8).

3.4 | The difference in GPR wave velocity and GPR energy attenuation in two seasons

The GPR images collected over the metal rebar by two antenna frequencies and in two seasons are compared in Figure 9. The GPR wave velocity increases from 0.142 m ns^{-1} (or 0.140 m ns^{-1}) in summer to 0.187 m ns^{-1} (or 0.184 m ns^{-1}) in winter for the 900 MHz (or 400 MHz) antenna frequency. After energy attenuation is compensated using the same gain factor in both seasons, the reflection amplitude is higher in winter, especially after 8 ns in the 900 MHz image (Figure 9c) and after 10 ns in the 400 MHz image (Figure 9f). The faster wave velocity and less GPR energy attenuation together lead to the deeper detection depth in winter for both antenna frequencies (Figures 4–8).

3.5 | Ground truthing

The detection frequency of the number of lateral coarse roots is compared between during the growing season

(August) and after the growing season (October) (Figure 10). A total of 96 (or 88) lateral coarse roots were documented in the excavation of six transects in August (or October). Root size, root depth and antenna frequency together determine the effectiveness of GPR in detecting lateral coarse roots. For example, roots with smaller diameters and deeper depths are more difficult to detect by GPR (Figure S1). The average detection frequency of the 900 MHz (or 400 MHz) GPR is 56.5% (or 50.7%) in August and 62.5% (or 59.1%) in October, suggesting consistent detection frequency between the two periods. Integration of root detection results of two antenna frequencies improves the detection frequency to 65.4% in August and 70.45% in October. The enhanced detection effectiveness by combining two antenna frequencies is most considerable in the deeper soil (0.6–0.9 m deep). Ground truthing data indicate that the 400 MHz GPR complements the 900 MHz GPR by detecting more roots in deeper soil, and the 900 MHz GPR complements the 400 MHz GPR by detecting more roots with smaller diameters at shallower depths (Figure 10). Because of site-specific conditions, the number and depth of roots in a root diameter class varied between survey lines, leading to some discrepancy in the detection frequency of the same diameter class in two surveys. Moreover, the observation on the natural outcropping of soil indicates no presence of non-root reflectors in the root zone (0–2 m depth), which ensures the high accuracy of root detection by GPR at the site (Figure 4e).

4 | DISCUSSION

Our results indicate that the 900 MHz antenna was more effective in detecting lateral coarse roots from the surface to 1 m depth, whereas the 400 MHz antenna revealed

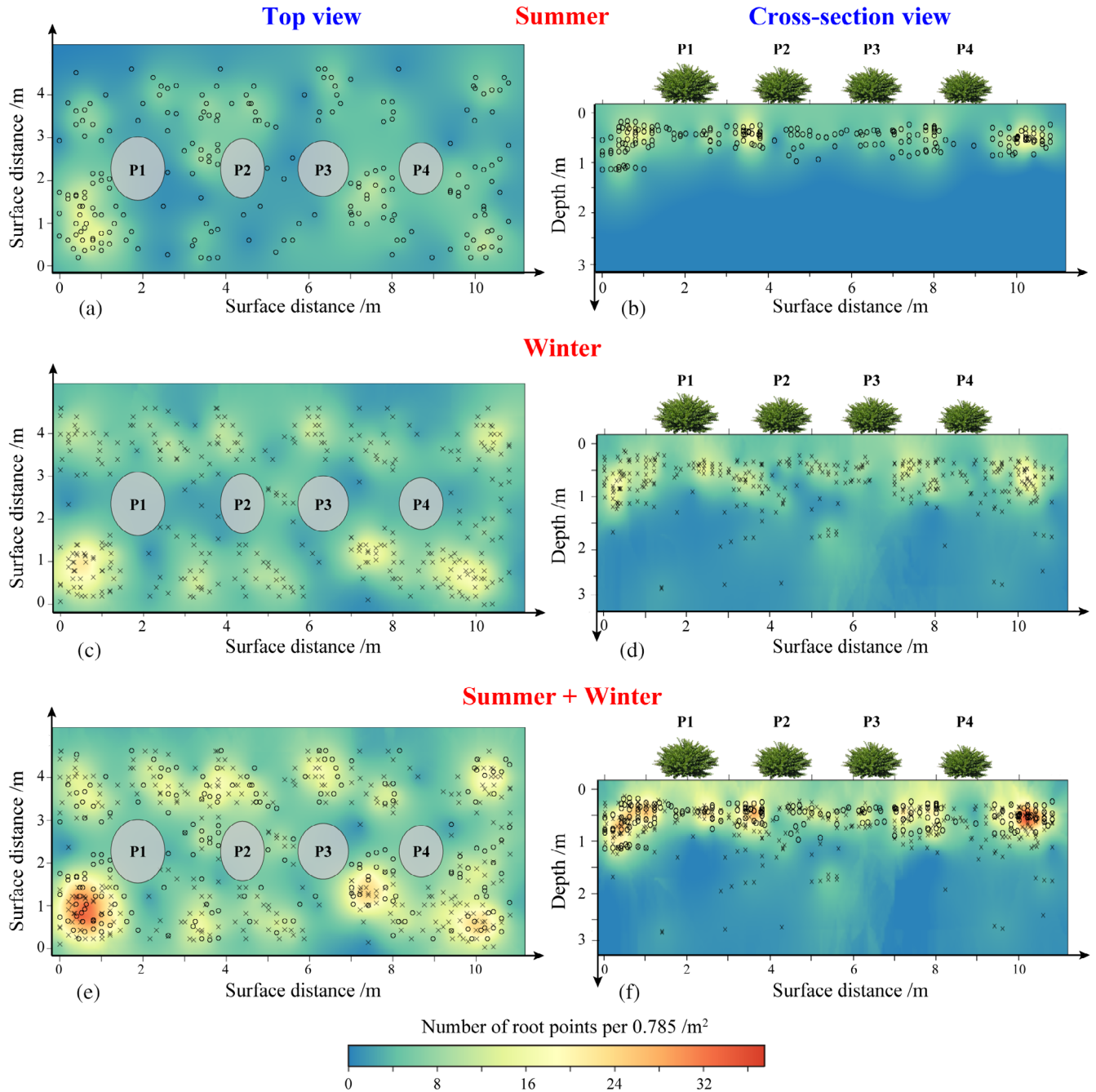


FIGURE 7 Spatial distribution of lateral coarse roots derived by the 400 MHz GPR in summer (a, b) and winter (c, d). The open circles (or crosses) indicate the roots identified in summer (or winter). The base map is the interpolated root distribution density. (e, f) Root distribution map after combining root detection results in summer and winter. Note that roots identified in summer and in both seasons are indicated by the open circles, and the cross marks indicate the roots only detected in winter. (a, c, e) The top view. (b, d, f) The cross-section view. P1–P4 indicates the shrubs within the GPR survey grid

more roots in the soil deeper than 1 m (Figure 6). Integration of root detection results obtained with a lower antenna frequency and a higher frequency allows a high detection resolution in the shallower soil and a deeper penetration than using a single antenna frequency (Figures 4–7). Previous studies reported that single-frequency GPR underestimated the number and biomass

of coarse roots under various field conditions (Butnor et al., 2016; Hirano et al., 2012). This study demonstrates the effectiveness of the dual-frequency GPR system in maximizing the detection frequency of coarse roots in sandy soils (Figure 8b). More field tests are needed to demonstrate the performance of the dual-frequency GPR in detecting coarse roots in other areas.

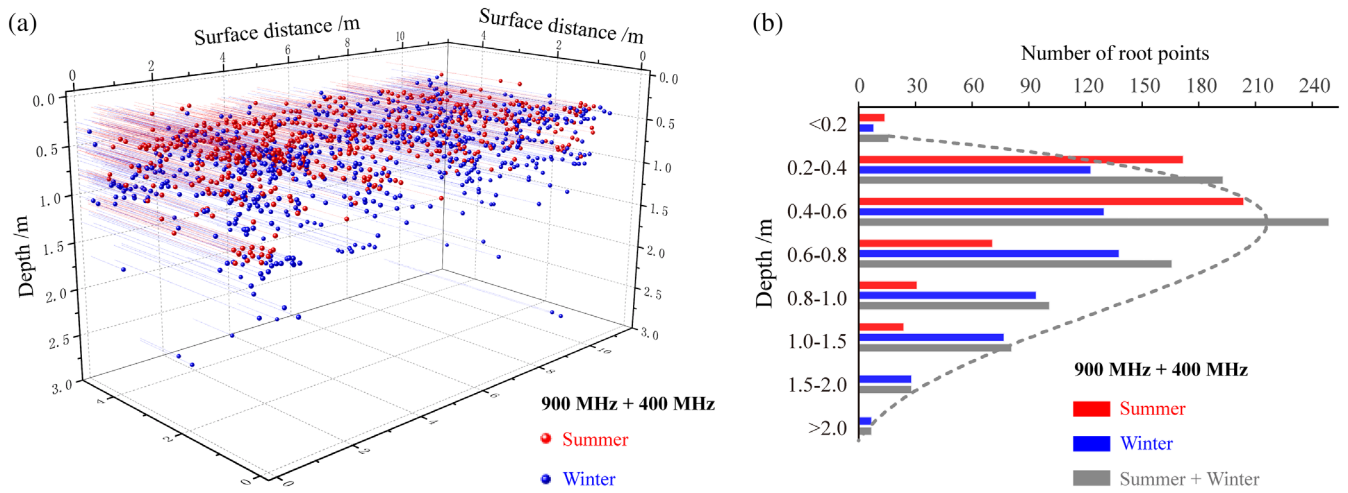


FIGURE 8 (a) Reconstructing the three-dimensional distribution of lateral coarse roots by combining GPR root detection results with two antenna frequencies and in two seasons. Note that the red dots indicate roots identified in summer and in both seasons, and the blue dots indicate the root points that are only identified in winter. (b) Root profile of the lateral coarse roots obtained in summer (red histograms), winter (blue histograms), and summer and winter combined (grey histograms)

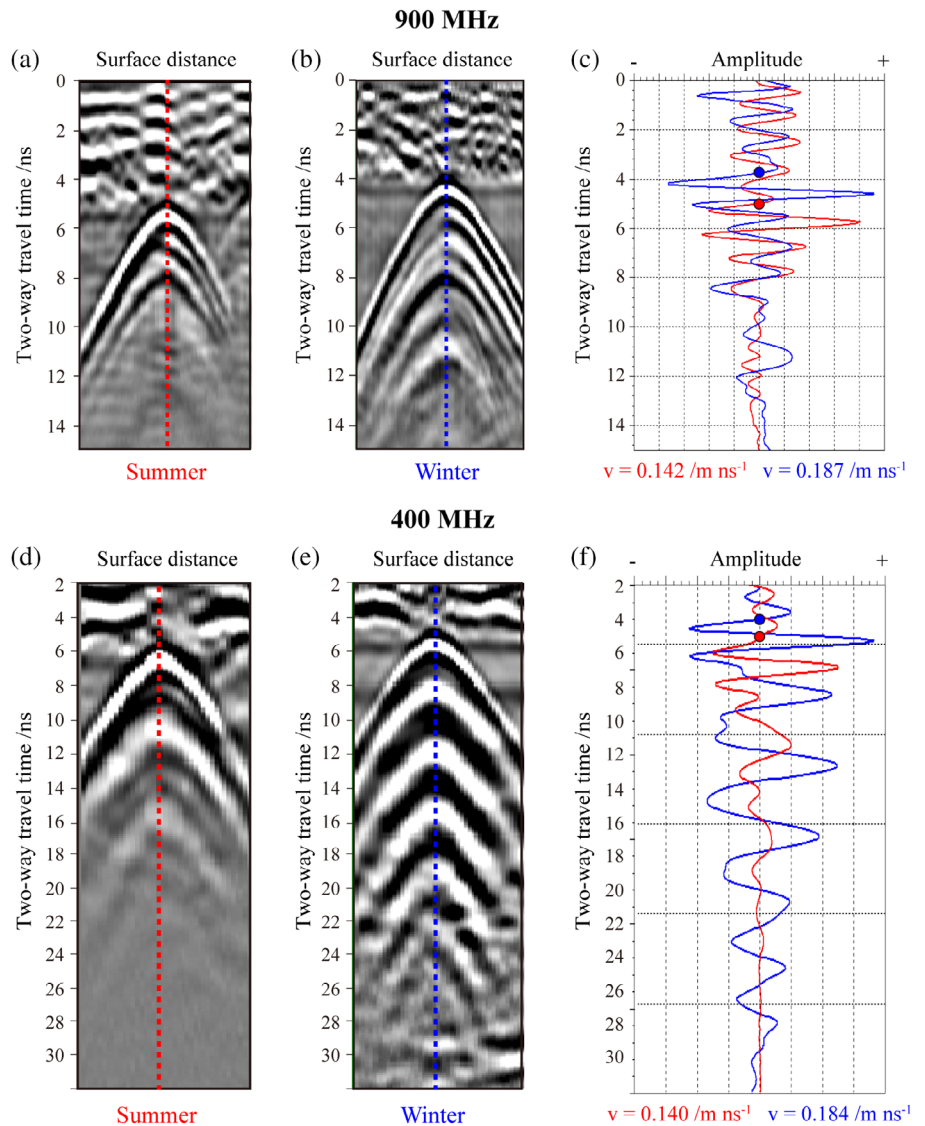


FIGURE 9 A comparison of GPR wave velocity and GPR energy attenuation between summer and winter. (a, b) GPR images of the buried metal reflector collected by the 900 MHz GPR. (c) The traces passing through the peak of the hyperbolic reflection as indicated by the vertical dashed lines in (a, b). The red (or blue) dot indicates the first break time of the GPR wave travelling from the antenna to the top of the metal reflector in summer (or winter); (d, e, f) are the same as (a, b, c) but for data collected by the 400 MHz GPR

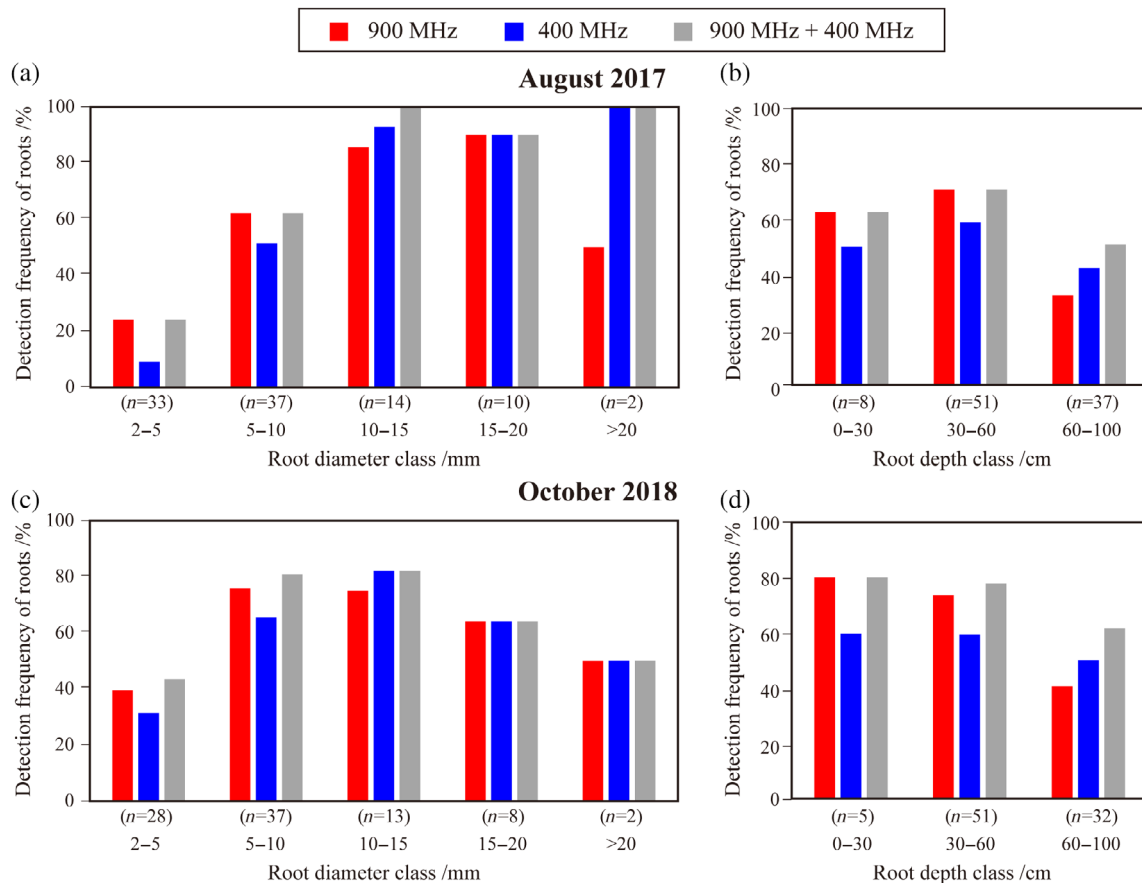


FIGURE 10 Detection frequency of the number of coarse roots in each root diameter class and root depth class obtained by ground truthing. N indicates the number of lateral coarse roots observed in the excavation in each root class. (a, b) Results of August 2017. (c, d) Results of October 2018. The red and blue bars indicate the detection frequency of 900 MHz and 400 MHz GPR, respectively. The grey bars indicate the detection frequency after combining root detection results of two antenna frequencies

Because the lower antenna frequency is more capable of probing subsurface stratification (e.g. soil layering patterns and the soil-bedrock surface) (Figure 4e), the dual-frequency GPR can gain more insight into the relationship between coarse root distribution and subsurface structures. This study provides such an example by showing that the presence of a caliche layer in the Calcic Kastanozems soil impedes the deep rooting of *C. microphylla* Lam. (Figure 4d, e). The caliche layer impeding deep rooting of shrubs in an arid environment has also been reported by Gile, Peterson, and Grossman (1966) and Li, Zhang, Peng, Hu, and Ma (2013). The consistency between root distribution patterns derived by two antenna frequencies also served as a cross-validation to help reliable interpretation of GPR data (Figures 5 and 7). Compared to conducting GPR surveys with a high antenna frequency and a low antenna frequency separately, the dual-frequency GPR system simultaneously collects data with two frequencies over the same survey line. This not only saves time and labour for data collection but also ensures the comparability between the GPR images collected with different antenna frequencies.

In addition to combining root detection results obtained by two antenna frequencies, we also paired GPR measurements under contrasting soil conditions (i.e. wetter soil in summer and frozen soil in winter) (Figures 5 and 7). To the best of our knowledge, this is the first time that repeated GPR surveys have been conducted to enhance GPR-based root detection. Many efforts have been made to apply repeated geophysical approaches to look for the temporal evolution and spatial distribution of soil moisture and subsurface flow (e.g. Guo et al., 2014; Steelman, Endres, & Jones, 2012). This study demonstrates the potential of repeated GPR surveys under different field conditions to maximize the detection frequency of coarse roots by GPR. In summer, the shrubs have a higher biological activity (e.g. stronger evapotranspiration and root water uptake to support shrub growth) (Figure 1c). The higher root moisture and, thus, the larger contrast in dielectric permittivity between coarse roots and the surrounding soil (Guo, Lin, et al., 2013) in summer may explain the higher detection frequency of coarse roots in the shallower soil in summer for both antenna frequencies (Figures 4 and 6). In

winter the soil is relatively drier than in summer (Table 1), which allows faster propagation of the GPR wave. When the liquid water transforms into ice, its dielectric constant decreases from ~80 to ~3 (Evans, 1965), which also elevates GPR wave velocity. Also, the electrical conductivity of water can decrease four orders of magnitude when it turns to ice (Liu, Gao, Han, Ma, & Gao, 2016). The much lower electrical conductivity of the frozen soil than the summer soil weakens the attenuation and dispersion of GPR energy (Jol, 2009). Therefore, the frozen soil has a faster wave velocity and less GPR energy attenuation and dispersion, which is favourable for a deeper detection range (Figures 4 and 6), and the integration of results of detection of coarse roots in summer and winter allows a higher detection frequency in both the shallow and deep soil (Figure 8). Similar to the comparison between two antenna frequencies, the correspondence of root distribution patterns in two seasonal surveys can be considered as cross-validation to constrain the interpretation of GPR results. Therefore, in addition to ground truthing via borehole data or excavation, which is destructive and laborious, GPR measurements with different antenna frequencies and under different field conditions can be coupled to enhance reliable and non-invasive investigation of coarse roots.

Through pairing the dual-frequency measurements in two seasons, we revealed the influence of microtopography (i.e. the surface depression area) and interplant root competition on the distribution of coarse roots in the survey area (Figures 5 and 7). Fewer lateral roots are distributed under the intershrub area (Figure 5a, c), which is likely to be a result of interplant root competition (Borden et al., 2017). The inhibition of interplant root overlap in shrub species was also reported in Mahall and Callaway (1992) and Schenk (1999). In addition, fewer lateral coarse roots are detected under the canopy, reflecting that lateral spread and branching of coarse roots under the canopy are limited for shrub species (Kummerow, Krause, & Jow, 1977; Schenk & Jackson, 2002). Because of the fast data acquisition rate of GPR (i.e. data collection for all 46 survey lines took about 2 hours), we believe that the GPR method can be applied to a larger spatial scale to determine the controls of coarse root distribution. The optimal distribution map of lateral coarse roots (Figure 8a) also benefits root biomass estimation (Butnor et al., 2016) and root system architecture reconstruction (Wu, Guo, Cui, et al., 2014) using the GPR method by adding more root points. Apart from seasonal surveys, the recent development in soil moisture mapping by GPR (Liu et al., 2019) makes it possible to compare the spatial pattern of soil moisture and coarse roots if GPR surveys are repeated for a period of several days after a rainfall. Given the increasing use of GPR in field root studies,

we expected broader applications of our experimental protocol to enhance the GPR-based root investigation.

5 | CONCLUSIONS

The dual-frequency GPR system (operating at 900 and 400 MHz) was tested for detecting and mapping lateral coarse roots of shrubs (*C. microphylla* Lam.) in sandy soils in the temperate semi-arid shrubland in China. Ground-penetrating radar surveys over a $4.8 \times 11 \text{ m}^2$ area were repeated in summer and winter with contrasting soil conditions. The lower antenna frequency detected more lateral coarse roots in the deeper soil due to a larger penetration depth, whereas the higher antenna frequency recognized more lateral coarse roots in the shallower soil due to the higher detection resolution. More lateral coarse roots were detected in the shallower soil in summer, probably because of a higher root water content. The frozen soil reduced the attenuation of GPR energy and was favourable for identifying coarse roots in the deeper soil. Pairing dual-frequency GPR measurements in two seasons revealed the influence of microtopography and interplant root competition on the spatial distribution of lateral coarse roots that was not evident in GPR images collected with a single frequency or a one-time survey. Ground truthing confirmed that pairing GPR data collected at two frequencies improved the detection frequency of the number of lateral coarse roots. More field tests are needed to enhance the application of the dual-frequency GPR and repeated GPR surveys in field root investigation under different site conditions.

ACKNOWLEDGEMENTS

This study was supported by the National Natural Science Foundation of China (Grant No. 41571404 and No. 41401378). The authors are thankful for the assistance in field data collection from Qixin Liu, Zhenxian Quan, Qi Dong, Chishan Zhang and Wenqing Wang. We also thank two anonymous reviewers, the Associate Editor (Paul Hallett) and the Editor-in-Chief (Jennifer Dungait) for their valuable comments and suggestions, which have helped improve the quality of this paper.

CONFLICTS OF INTEREST

The authors declare that they have no conflict of interests.

DATA AVAILABILITY STATEMENT

The data that support the findings of this study are available from the corresponding author upon reasonable request.

ORCID

L. Guo  <https://orcid.org/0000-0003-3821-4058>

REFERENCES

- al Hagrey, S. A. (2007). Geophysical imaging of root-zone, trunk, and moisture heterogeneity. *Journal of Experimental Botany*, *58*, 839–854.
- Angermann, L., Jackisch, C., Allroggen, N., Sprenger, M., Zehe, E., Tronicke, J., ... Blume, T. (2017). Form and function in hillslope hydrology: Characterization of subsurface flow based on response observations. *Hydrology and Earth System Sciences*, *21*, 3727–3748.
- Berling, D. J., & Berner, R. A. (2005). Feedbacks and the coevolution of plants and atmospheric CO₂. *Proceedings of the National Academy of Sciences of the United States of America*, *102*, 1302–1305.
- Borden, K. A., Thomas, S. C., & Isaac, M. E. (2017). Interspecific variation of tree root architecture in a temperate agroforestry system characterized using ground-penetrating radar. *Plant and Soil*, *410*, 323–334.
- Brantley, S. L., Eissenstat, D. M., Marshall, J. A., Godsey, S. E., Balogh-Brunstad, Z., Karwan, D. L., ... Weathers, K. C. (2017). Reviews and syntheses: On the roles trees play in building and plumbing the critical zone. *Biogeosciences*, *14*, 5115–5142.
- Brassard, B. W., Chen, H. Y. H., Bergeron, Y., & Pare, D. (2011). Coarse root biomass allometric equations for *Abies balsamea*, *Picea mariana*, *Pinus banksiana*, and *Populus tremuloides* in the boreal forest of Ontario, Canada. *Biomass & Bioenergy*, *35*, 4189–4196.
- Butnor, J. R., Doolittle, J. A., Johnsen, K. H., Samuelson, L., Stokes, T., & Kress, L. (2003). Utility of ground-penetrating radar as a root biomass survey tool in forest systems. *Soil Science Society of America Journal*, *67*, 1607–1615.
- Butnor, J. R., Samuelson, L. J., Stokes, T. A., Johnsen, K. H., Anderson, P. H., & Gonzalez-Benecke, C. A. (2016). Surface-based GPR underestimates below-stump root biomass. *Plant and Soil*, *402*, 47–62.
- Cao, X., Liu, Y., Liu, Q. X., Cui, X. H., Chen, X. H., & Chen, J. (2018). Estimating the age and population structure of encroaching shrubs in arid/semiarid grasslands using high spatial resolution remote sensing imagery. *Remote Sensing of Environment*, *216*, 572–585.
- Chen, J., Hori, Y., Yamamura, Y., Shiyomi, M., & Huang, D. M. (2008). Spatial heterogeneity and diversity analysis of macro-vegetation in the Xilingol region, Inner Mongolia, China, using the beta distribution. *Journal of Arid Environments*, *72*, 1110–1119.
- Chi, D. K., Wang, H., Li, X. B., Liu, H. H., & Li, X. H. (2018). Assessing the effects of grazing on variations of vegetation NPP in the Xilingol grassland, China, using a grazing pressure index. *Ecological Indicators*, *88*, 372–383.
- De Coster, A., & Lambot, E. (2018). Fusion of multifrequency GPR data freed from antenna effects. *Ieee Journal of Selected Topics in Applied Earth Observations and Remote Sensing*, *11*, 664–674.
- Deans, J. D. (1981). Dynamics of coarse root production in a young plantation of *Picea-Sitchensis*. *Forestry*, *54*, 139–155.
- Ennos, A. R. (1993). The scaling of root anchorage. *Journal of Theoretical Biology*, *161*, 61–75.
- Evans, S. (1965). Dielectric properties of ice and snow - a review. *Journal of Glaciology*, *5*, 773–793.
- Fan, Y., Miguez-Macho, G., Jobbagy, E. G., Jackson, R. B., & Otero-Casal, C. (2017). Hydrologic regulation of plant rooting depth. *Proceedings of the National Academy of Sciences of the United States of America*, *114*, 10572–10577.
- Gile, L. H., Peterson, F. F., & Grossman, R. B. (1966). Morphological and genetic sequences of carbonate accumulation in desert soils. *Soil Science*, *101*, 347–360.
- Guo, L., Chen, J., Cui, X. H., Fan, B. H., & Lin, H. (2013). Application of ground penetrating radar for coarse root detection and quantification: A review. *Plant and Soil*, *362*, 1–23.
- Guo, L., Chen, J., & Lin, H. (2014). Subsurface lateral preferential flow network revealed by time-lapse ground-penetrating radar in a hillslope. *Water Resources Research*, *50*, 9127–9147.
- Guo, L., & Lin, H. (2018). Addressing two bottlenecks to advance the understanding of preferential flow in soils. *Advances in Agronomy*, *147*, 61–117.
- Guo, L., Lin, H., Fan, B., Cui, X., & Chen, J. (2013). Impact of root water content on root biomass estimation using ground penetrating radar: Evidence from forward simulations and field controlled experiments. *Plant and Soil*, *371*, 503–520.
- Guo, L., Wu, Y., Chen, J., Hirano, Y., Tanikawa, T., Li, W., & Cui, X. (2015). Calibrating the impact of root orientation on root quantification using ground-penetrating radar. *Plant and Soil*, *395*, 289–305.
- Hirano, Y., Dannoura, M., Aono, K., Igarashi, T., Ishii, M., Yamase, K., ... Kanazawa, Y. (2009). Limiting factors in the detection of tree roots using ground-penetrating radar. *Plant and Soil*, *319*, 15–24.
- Hirano, Y., Yamamoto, R., Dannoura, M., Aono, K., Igarashi, T., Ishii, M., ... Kanazawa, Y. (2012). Detection frequency of *Pinus thunbergii* roots by ground-penetrating radar is related to root biomass. *Plant and Soil*, *360*, 363–373.
- Hoffmann, C., Funk, R., Reiche, M., & Li, Y. (2011). Assessment of extreme wind erosion and its impacts in Inner Mongolia, China. *Aeolian Research*, *3*, 343–351.
- Hugenschmidt, J., & Kalogeropoulos, A. (2009). The inspection of retaining walls using GPR. *Journal of Applied Geophysics*, *67*, 335–344.
- Huisman, J. A., Hubbard, S. S., Redman, J. D., & Annan, A. P. (2003). Measuring soil water content with ground penetrating radar: A review. *Vadose Zone Journal*, *2*, 476–491.
- Jackson, R. B., Canadell, J., Ehleringer, J. R., Mooney, H. A., Sala, O. E., & Schulze, E. D. (1996). A global analysis of root distributions for terrestrial biomes. *Oecologia*, *108*, 389–411.
- Jayawickreme, D. H., Jobbagy, E. G., & Jackson, R. B. (2014). Geophysical subsurface imaging for ecological applications. *New Phytologist*, *201*, 1170–1175.
- Jol, H. M. (2009). *Ground penetrating radar theory and applications*. Amsterdam: Elsevier.
- Klenk, P., Jaumann, S., & Roth, K. (2015). Monitoring infiltration processes with high-resolution surface-based ground-penetrating radar. *Hydrology and Earth System Sciences Discussion*, *12*, 12215–12246.
- Kummerow, J., Krause, D., & Jow, W. (1977). Root systems of chaparral shrubs. *Oecologia*, *29*, 163–177.

- Leucci, G. (2010). The use of three geophysical methods for 3D images of total root volume of soil in urban environments. *Exploration Geophysics*, *41*, 268–278.
- Li, W. T., Cui, X. H., Guo, L., Chen, J., Chen, X. H., & Cao, X. (2016). Tree root automatic recognition in ground penetrating radar profiles based on randomized Hough transform. *Remote Sensing*, *8*, 1–11.
- Li, X. Y., Hu, X., Zhang, Z. H., Peng, H. Y., Zhang, S. Y., Li, G. Y., ... Ma, Y. J. (2013). Shrub hydrogeology: Preferential water availability to deep soil layer. *Vadose Zone Journal*, *12*, 1–12.
- Li, X. Y., Yang, Z. P., Li, Y. T., & Lin, H. (2009). Connecting ecohydrology and hydrogeology in desert shrubs: Stemflow as a source of preferential flow in soils. *Hydrology and Earth System Sciences*, *13*, 1133–1144.
- Li, X. Y., Zhang, S. Y., Peng, H. Y., Hu, X., & Ma, Y. J. (2013). Soil water and temperature dynamics in shrub-encroached grasslands and climatic implications: Results from Inner Mongolia steppe ecosystem of North China. *Agricultural and Forest Meteorology*, *171*, 20–30.
- Liu, B., Gao, Y., Han, Y. H., Ma, Y. Z., & Gao, C. X. (2016). In situ electrical conductivity measurements of H₂O under static pressure up to 28 GPa. *Physics Letters A*, *380*, 2979–2983.
- Liu, X. B., Cui, X. H., Guo, L., Chen, J., Li, W. T., Yang, D. D., ... Lin, H. (2019). Non-invasive estimation of root zone soil moisture from coarse root reflections in ground-penetrating radar images. *Plant and Soil*, *436*, 623–639.
- Liu, X. W., Dong, X. J., Xue, Q. W., Leskovar, D. I., Jifon, J., Butnor, J. R., & Marek, T. (2018). Ground penetrating radar (GPR) detects fine roots of agricultural crops in the field. *Plant and Soil*, *423*, 517–531.
- Mahall, B. E., & Callaway, R. M. (1992). Root communication mechanisms and intracommunity distributions of 2 Mojave desert shrubs. *Ecology*, *73*, 2145–2151.
- Millikin, C. S., & Bledsoe, C. S. (1999). Biomass and distribution of fine and coarse roots from blue oak (*Quercus douglasii*) trees in the northern Sierra Nevada foothills of California. *Plant and Soil*, *214*, 27–38.
- Molon, M., Boyce, J. I., & Arain, M. A. (2017). Quantitative, nondestructive estimates of coarse root biomass in a temperate pine forest using 3-D ground-penetrating radar (GPR). *Journal of Geophysical Research-Biogeosciences*, *122*, 80–102.
- Noguchi, S., Tsuboyama, Y., Sidle, R. C., & Hosoda, I. (1999). Morphological characteristics of macropores and the distribution of preferential flow pathways in a forested slope segment. *Soil Science Society of America Journal*, *63*, 1413–1423.
- Parsekian, A. D., Singha, K., Minsley, B. J., Holbrook, W. S., & Slater, L. (2015). Multiscale geophysical imaging of the critical zone. *Reviews of Geophysics*, *53*, 1–26.
- Raz-Yaseef, N., Koteen, L., & Baldocchi, D. D. (2013). Coarse root distribution of a semi-arid oak savanna estimated with ground penetrating radar. *Journal of Geophysical Research-Biogeosciences*, *118*, 135–147.
- Ren, H. R., & Zhang, B. (2018). Spatiotemporal variations in litter mass and their relationships with climate in temperate grassland: A case study from Xilingol grassland, Inner Mongolia (China). *Advances in Space Research*, *61*, 1055–1065.
- Resh, S. C., Battaglia, M., Worledge, D., & Ladiges, S. (2003). Coarse root biomass for eucalypt plantations in Tasmania, Australia: Sources of variation and methods for assessment. *Trees*, *17*, 389–399.
- Reubens, B., Poesen, J., Danjon, F., Geudens, G., & Muys, B. (2007). The role of fine and coarse roots in shallow slope stability and soil erosion control with a focus on root system architecture: A review. *Trees*, *21*, 385–402.
- Schenk, H. J. (1999). Clonal splitting in desert shrubs. *Plant Ecology*, *141*, 41–52.
- Schenk, H. J., & Jackson, R. B. (2002). Rooting depths, lateral root spreads and below-ground/above-ground allometries of plants in water-limited ecosystems. *Journal of Ecology*, *90*, 480–494.
- Steelman, C. M., Endres, A. L., & Jones, J. P. (2012). High-resolution ground-penetrating radar monitoring of soil moisture dynamics: Field results, interpretation, and comparison with unsaturated flow model. *Water Resources Research*, *48*, 1–18.
- Tamura, K., Asano, M., & Jamsran, U. (2013). Soil diversity in Mongolia. In N. Yamamura, N. Fujita, & A. Maekawa (Eds.), *The Mongolian ecosystem network: Environmental issues under climate and social changes* (pp. 99–103). Japan, Tokyo: Springer.
- Topp, G. C., Davis, J. L., & Annan, A. P. (1980). Electromagnetic determination of soil-water content - measurements in coaxial transmission-lines. *Water Resources Research*, *16*, 574–582.
- Wu, J. G., Naeem, S., Elser, J., Bai, Y. F., Huang, J. H., Kang, L., ... Han, X. G. (2015). Testing biodiversity-ecosystem functioning relationship in the world's largest grassland: Overview of the IMGRE project. *Landscape Ecology*, *30*, 1723–1736.
- Wu, Y., Guo, L., Cui, X., Chen, J., Cao, X., & Lin, H. (2014). Ground-penetrating radar-based automatic reconstruction of three-dimensional coarse root system architecture. *Plant and Soil*, *383*, 155–172.
- Wu, Y., Guo, L., Li, W., Cui, X., & Chen, J. (2014). Comment on: "root orientation can affect detection accuracy of ground-penetrating radar". *Plant and Soil*, *380*, 441–444.
- Xiao, J. & Liu, L. 2015. Multi-frequency GPR signal fusion using forward and inverse S-transform for detecting railway subgrade defects, 2015 8th International Workshop on Advanced Ground Penetrating Radar (IWAGPR), pp. 1-4.
- Yi, R., Shiyomi, M., Akiyama, T., Wang, S., Yamamura, Y., Hori, Y., & Ai, L. (2014). Long-term prediction of grassland production for five temporal patterns of precipitation during the growing season of plants based on a system model in Xilingol, Inner Mongolia, China. *Ecological Modelling*, *291*, 183–192.
- Zhang, Z. H., Li, X. Y., Jiang, Z. Y., Peng, H. Y., Li, L., & Zhao, G. Q. (2013). Changes in some soil properties induced by re-conversion of cropland into grassland in the semiarid steppe zone of Inner Mongolia, China. *Plant and Soil*, *373*, 89–106.
- Zhao, Y., Peth, S., Hallett, P., Wang, X. Y., Giese, M., Gao, Y. Z., & Horn, R. (2011). Factors controlling the spatial patterns of soil moisture in a grazed semi-arid steppe investigated by multivariate geostatistics. *Ecohydrology*, *4*, 36–48.
- Zhao, Y., Peth, S., Wang, X. Y., Lin, H., & Horn, R. (2010). Controls of surface soil moisture spatial patterns and their temporal stability in a semi-arid steppe. *Hydrological Processes*, *24*, 2507–2519.

Zhu, S. P., Huang, C. L., Su, Y., & Sato, M. (2014). 3D ground penetrating radar to detect tree roots and estimate root biomass in the field. *Remote Sensing*, *6*, 5754–5773.

SUPPORTING INFORMATION

Additional supporting information may be found online in the Supporting Information section at the end of this article.

How to cite this article: Cui X, Liu X, Cao X, et al. Pairing dual-frequency GPR in summer and winter enhances the detection and mapping of coarse roots in the semi-arid shrubland in China. *Eur J Soil Sci.* 2019;1–16. <https://doi.org/10.1111/ejss.12858>